Journal of Orthopaedic Research®

WILEY | ORS Orthopaedic Research Society

RESEARCH ARTICLE

Cartilage

The Influence of the Chondrocyte Microenvironment on Multiscale Articular Cartilage Mechanics: A Computational Study

Malek Adouni[1] | Afif Gouissem[2] | Tanvir Faisal[3] | Yasin Y. Dhaher[4,5,6,7]

[1]Abdullah Al Salem University, Biomedical and Instrumentation Engineering, Khalidiya, Kuwait | [2]Mechanical Engineering department, Australian University of Kuwait, Mubarak Al-Abdullah, Kuwait | [3]Department of Mechanical Engineering, University of Louisiana at Lafayette, Lafayette, LA, USA | [4]Physical Medicine and Rehabilitation Department, Northwestern University, Chicago, IL, USA | [5]Department of Physical Medicine and Rehabilitation, University of Texas Southwest, Dallas, TX, USA | [6]Department of Orthopedic Surgery, University of Texas Southwest, Dallas, TX, USA | [7]Bioengineering, University of Texas Southwest, Dallas, TX, USA

Correspondence: Malek Adouni (malek.adouni@polymtl.ca; malek.adouni@gmail.com)

Received: 11 February 2026 | **Revised:** 11 May 2026 | **Accepted:** 3 July 2026

Funding: Kuwait Foundation for the Advancement of Sciences, Grant/Award Number: CN22-13BP-1706

Keywords: articular cartilage | chondrocyte | collagen VI | finite element analysis | mechanotransduction | multiscale modeling | pericellular matrix (PCM)

ABSTRACT

Chondrocytes are mechanosensitive cells whose biosynthetic activity is governed by their local mechanical environment within articular cartilage. This environment is strongly influenced by the pericellular matrix (PCM), a specialized region enriched in collagen VI and a distinct non-fibrillar ground substance. However, the individual mechanical roles of these PCM constituents in regulating chondrocyte mechanotransduction remain poorly understood. In this study, an explicit, concurrent multiscale finite element model of articular cartilage was developed to directly link tissue-level loading to cellular-scale mechanics. The model incorporates anatomically realistic chondrocyte distributions, depth-dependent collagen II fibril architecture, and distinct representations of collagen VI fibrils and the non-fibrillar PCM matrix. Unconfined compression simulations were performed under reference conditions and following targeted alterations (±20%) in collagen VI stiffness, PCM matrix stiffness, or both. Results showed that tissue-level reaction forces were most sensitive to collagen VI stiffness. At the cellular scale, changes in collagen VI and PCM matrix properties significantly modulated chondrocyte circumferential forces and volumetric deformation, particularly in the superficial zone. Stress redistribution analyses revealed a load-sharing mechanism between fibrillar and non-fibrillar PCM components. These findings clarify the distinct mechanical roles of PCM constituents and provide mechanistic insight into how their degradation may disrupt chondrocyte mechanotransduction and contribute to cartilage degeneration.

1 | Introduction

Articular cartilage is a specialized connective tissue that enables near-frictionless articulation and load distribution in synovial joints. Its functional integrity relies on a complex, hierarchical structure comprising a sparse population of chondrocytes embedded within a dense extracellular matrix (ECM) [1]. The chondrocyte's immediate mechanical environment is stratified into specialized domains: the pericellular matrix (PCM), the territorial matrix (TM), and the interterritorial ECM [2, 3]. These domains differ in composition, particularly in collagen isoform prevalence. While collagen II dominates the ECM, the PCM is uniquely enriched with collagen VI and has a distinct proteoglycan composition, forming a critical interface that filters mechanical signals to the cell [4, 5].

The process by which chondrocytes convert mechanical stimuli into biochemical activity, mechanotransduction, is fundamental to cartilage homeostasis and pathology [6, 7]. Aberrant mechanotransduction is implicated in the onset and progression of osteoarthritis (OA) [8, 9]. The PCM is postulated to be a primary mechanosensory element, modulating the magnitude and type of mechanical stimuli (stress, strain, fluid flow, osmolarity) reaching the cell surface [4, 10]. Collagen VI, a major structural component of the PCM, forms a microfilamentous network that anchors the chondron to the broader ECM [11, 12]. Mutations or degradation of collagen VI are associated with altered chondrocyte mechanics and cartilage pathology [13, 14]. Similarly, changes in the composition and stiffness of the non-fibrillar PCM ground substance-rich in proteoglycans like aggrecan and perlecan-can influence local hydration, permeability, and stress distribution [15, 16].

Despite its importance, dissecting the individual mechanical contributions of the PCM's fibrillar (collagen VI) and non-fibrillar components "in vivo" is experimentally challenging due to the coupled nature of cartilage mechanics across scales. Computational modeling provides a powerful alternative to probe these relationships. Previous models have employed homogenization or post-processing sub-modeling techniques to bridge scales [17, 18]. While informative, these approaches can involve assumptions about scale separation or may not fully capture the continuous, reciprocal mechanical interactions between a large population of cells and their surrounding matrix under perturbation.

To overcome these limitations, this study presents an explicit, concurrent multiscale finite element model of articular cartilage in which tissue-scale and cell-scale mechanics are solved simultaneously within a single computational domain. Unlike homogenized or sequential sub-modeling approaches, this framework preserves continuous mechanical interactions between a large population of anatomically distributed chondrocytes and their surrounding matrix under loading. The model explicitly distinguishes between the fibrillar collagen VI network and the non-fibrillar ground substance of the PCM, enabling independent modulation of their mechanical properties. Using this framework, we test the hypothesis that collagen VI stiffness and PCM matrix stiffness have distinct and quantifiable effects on both aggregate tissue response and chondrocyte-level mechanical stimuli under unconfined compression. Isolated and combined alterations (±20%) in these PCM constituents are examined to elucidate their respective roles in load transfer and mechanotransduction.

2 | Methods

2.1 | Explicit Multiscale Finite-Element Model

An axisymmetric finite element model of an articular cartilage explant (diameter: 2.8 mm, height: 1.2 mm) was developed in Abaqus/Standard (2019, Dassault Systèmes). The model explicitly represents thousands of chondrocytes with their surrounding PCM, TM, and ECM, avoiding scale-separation assumptions. Construction occurred in three stages:

1. Micro-unit generation: Two 2D axisymmetric micro-units (800 μm^2) were created: a Cellular Unit (CCU) containing an ellipsoidal chondrocyte (dimensions based on histological data [2, 9, 19]; Table 1) surrounded by concentric PCM (~3 μm) and TM (~1 μm) layers, and a Non-Cellular Unit (CNU) of pure ECM (Figure 1). For consistency across all parametric scenarios, a uniform mildly oblate ellipsoidal cell geometry (based on mean dimensions from Youn et al. [19]) was applied across all depth zones. While experimental data confirm that chondrocyte morphology transitions from highly flattened in the superficial zone to near-spherical in the deep zone [19], using a single representative geometry across zones isolates the mechanical effects of the depth-varying fibril architecture, cell density, and material gradients, the primary variables under investigation, from confounding morphological variation. The sensitivity of predicted cellular outputs to zone-specific chondrocyte morphology is acknowledged as a target for future model refinement (see Limitations).
2. Periodic unit assembly using a nodal merging ("tiling") algorithm, CCUs and CNUs were assembled into a larger Periodic Unit (CPU, 3200 μm^2) that reflected the depth-dependent cell density and orientation observed in cartilage (Figure 2) (superficial: 75%, transitional: ~40%, deep: 12.5%). These cell density fractions are distributed across the following zonal depth proportions of the total tissue height: superficial zone (~10%–15%), transitional zone (~40%–45%), and deep zone (~40%–50%), consistent with histological measurements [13, 21] and annotated on Figure 2. [21].
3. Macro-model construction: The full explant model was generated by tiling the CPU, resulting in a seamless mesh with explicit representation of ~561 chondrocytes and their microenvironments. A non-porous, rigid indenter and subchondral bone were modeled as impermeable boundaries [20] (Figure 2).

Mesh Convergence: A mesh convergence study was performed prior to finalizing the model. Three refinement levels were evaluated for the representative periodic unit: a coarse mesh (~12,000 elements), an intermediate mesh (~28,000 elements), and the final fine mesh (~52,000 elements). Convergence was assessed using three output metrics: peak axial reaction force, chondrocyte circumferential force (superficial zone), and peak von Mises stress in the PCM. The coarse mesh yielded deviations of ~9%–11% relative to the fine mesh in cellular-level

TABLE 1 | CCU and CNU dimension in μm over cartilage layers [2, 9, 19].

	a [9, 19]	b [9, 19]	c [19]	d [19]	e [2, 19]	f [2, 19]
Superficial	8	16	12	24	40	20
Transitional	12	16	16	24	40	20
Deep	16	8	24	12	40	40

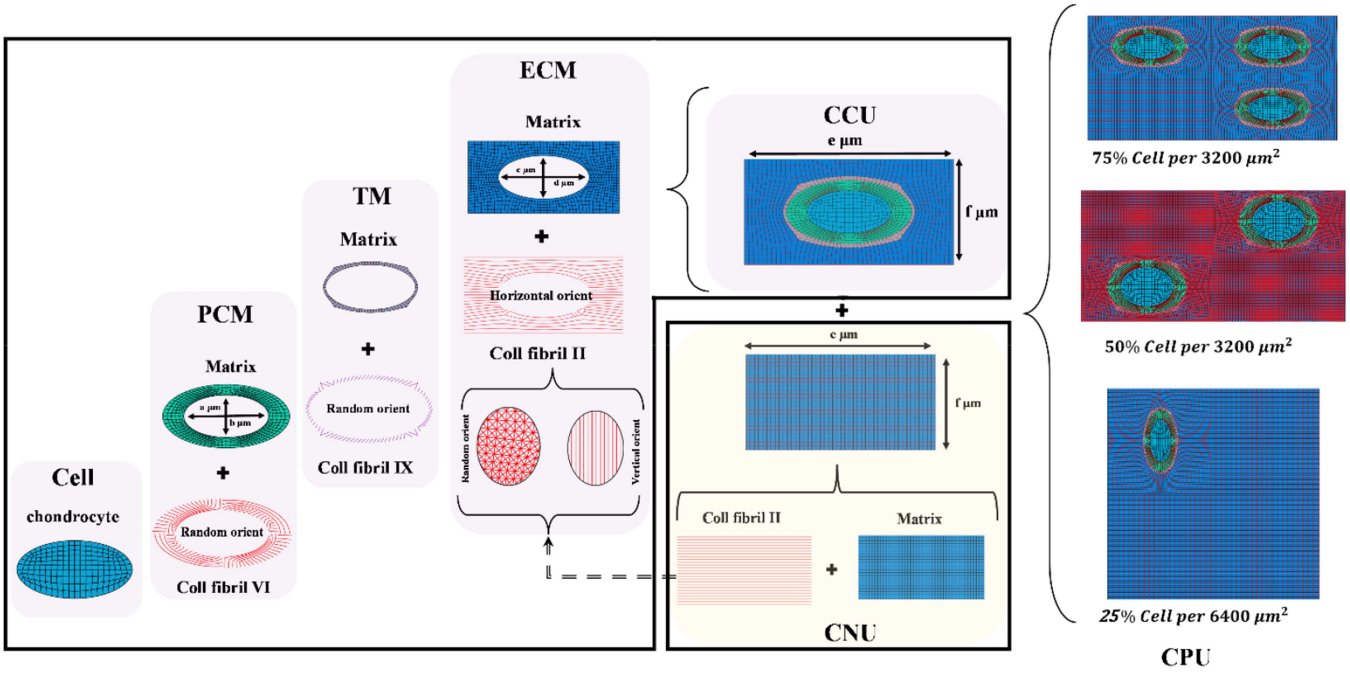

FIGURE 1 | Detailed mesh showing the distinct structures representing solid matrix and collagen fibril networks in the two 2D micro models, cartilage cellular unit (CCU) with chondrocyte and cartilage noncellular unit (CNU) without chondrocytes, and the cartilage periodic unit (CPU) in the different depth-dependent zones of the articular cartilage. Only collagen II has a different orientation over the depth, horizontal at the superficial zone, random at the transitional zone, and vertical at the deep zone. Dimensions of CCU and CNU are presented in Table 1.

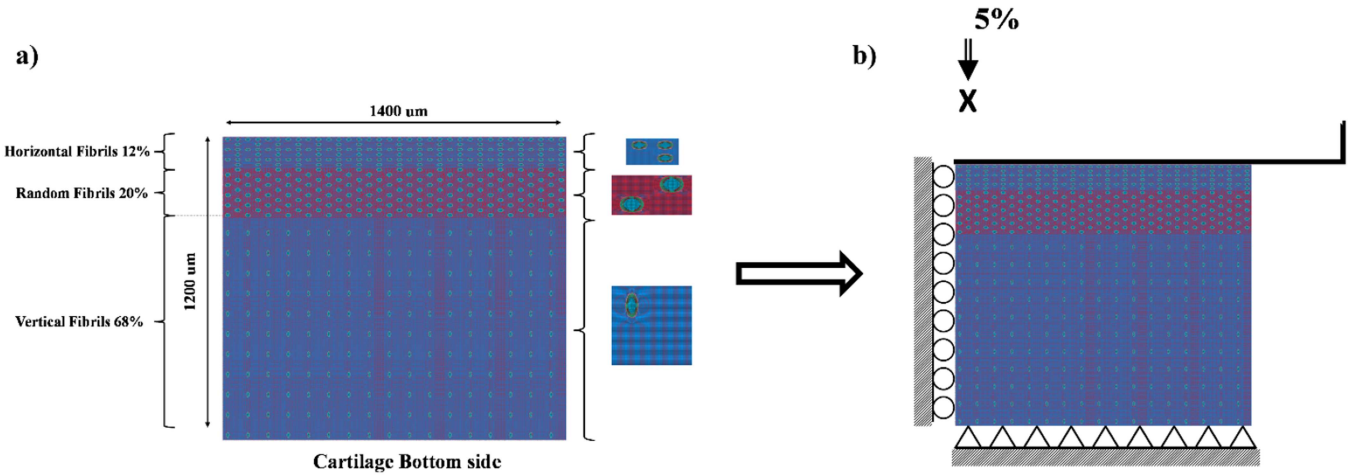

FIGURE 2 | Axisymmetric model of the articular cartilage (a) along with nonporous rigid indenter and testing paradigms (b) considered during this investigation to simulate the experimental work of DiSilvestro and Suh [20]. The model explicitly represents three depth-dependent zones: the superficial zone (~10%–15% of total tissue height; cell volume fraction 75%; horizontal collagen II orientation), the transitional zone (~40%–45%; ~40% cellular; random fibril orientation), and the deep zone (~40%–50%; 12.5% cellular; vertical collagen II orientation), consistent with histological measurements [13, 21]. These zonal boundaries and their associated cell density fractions are annotated on the figure.

outputs, while differences between the intermediate and fine meshes were less than 3.5% across all metrics. The fine mesh was therefore selected as it provided sufficient numerical accuracy while remaining computationally tractable for a model explicitly representing ~561 chondrocyte microenvironments.

The ECM, TM, and PCM were modeled as porous, hyperelastic solids (8-node, pore pressure elements, CAX8RP) reinforced by embedded tension-only fibrillar networks (membrane elements, MAX1) [22–24]. Collagen II fibrils in the ECM were assigned depth-dependent orientations: horizontal in the superficial zone, random in the transitional zone, and vertical in the deep zone [25]. Collagen VI and IX fibrils in the PCM and the TM respectively, were modeled with a random in-plane orientation [2, 3, 19, 26].

2.2 | Material Properties

The constitutive behavior incorporated three key nonlinearities:

1. Fibrillar Networks: A nonlinear stress-strain law defined fibril stress (σ^f) [27]:

$$\sigma^f = \frac{\eta_0^s}{J}\ln(\varepsilon_f)\left(E_0\varepsilon_f + E_\varepsilon\varepsilon_f^2\right) \text{ for } \varepsilon_f > 0$$

where (E_0) and (E_ε) are initial and strain-stiffening coefficients, (ε_f) is the logarithmic fibril strain, (η_0^s) is the initial solid volume fraction, and (J) is the volumetric Jacobian.

2. Non-fibrillar matrices: A compressible, edited neo-Hookean model combined with a swelling stress term defined the solid matrix stress (σ^{Mat}) [27, 28]:

$$\sigma^{Mat} = \eta_0^s\left[-\frac{\ln J}{6J}G_m\left(\frac{3\eta_0^s\ln J}{\eta_0^s - 1} - 3\frac{J+\eta_0^s}{J-\eta_0^s} - 1\right)I + \frac{G_m}{J}(FF^T - J^{2/3}I)\right] - \alpha_1 J^{-\alpha_2}I - pI$$

where (G_m) is the shear modulus, (F) is the deformation gradient, and (α_1, α_2) are swelling coefficients.

3. Strain-dependent permeability: Permeability (k) varied with void ratio (e) [29, 30]:

$$k = k_0\left(\frac{1+e}{1+e_0}\right)^M$$

The initial void ratio (e_0) decreased with depth from the articular surface to the subchondral bone [30]. The fluid fraction decreases in the model from 85% at the surface to 70% at the bone junction [31, 32].

Depth-dependent material parameters for the ECM (Collagen II) were adopted from prior validated models [26, 31, 32] (Table 2). Properties for the cell, PCM (collagen VI and non-fibrillar matrix), and TM were scaled from ECM values based on literature reports [3, 4, 15, 18, 26, 27, 31, 33, 34] (Table 3). All constitutive models were implemented via user subroutines (UMAT, ORIENT, VOIDRI).

2.3 | Loading, Boundary Conditions, and Study Cases

The simulation replicated an experimental unconfined compression test [20]: a 5% nominal strain was applied to the explant surface at a rate of 0.001/s, followed by stress relaxation. The subchondral bone was fixed and impermeable; the lateral surface was free-draining.

Pre-Swelling Equilibration: Prior to the mechanical compression protocol, a pre-swelling equilibration step was performed to establish physiologically consistent initial conditions. An osmotic pressure differential, governed by the depth-dependent swelling coefficients α_1 and α_2 in Equation (2), was applied in the absence of external mechanical load, with free-swelling boundary conditions at the lateral surface and zero applied displacement. The model was allowed to reach osmotic equilibrium, yielding a pre-stressed reference configuration in which collagen fibrils sustain an initial tensile pre-stress that counterbalances the proteoglycan-driven swelling pressure [27, 28]. This equilibrated configuration serves as the reference geometry for all subsequent mechanical loading simulations. Without this step, fibrils would be recruited from a zero-stress state, which would underestimate peak fibril stresses and tissue stiffness, particularly in the superficial zone where horizontal fibril tension is central to the compressive response. The swelling coefficients were held constant across all parametric scenarios (Ref, COLL(VI) ± 20%, PCM ± 20%), ensuring that the pre-swelling reference state was identical for all comparative simulations.

To investigate the role of PCM constituents, material properties were altered from the reference (Ref) case in three separate scenarios:

- COLL(VI) ± 20%: The linear (E_0) and nonlinear (E_ε) stiffness parameters of collagen VI fibrils were increased or decreased by 20%.
- PCM ± 20%: The shear modulus (G_m) of the non-fibrillar PCM solid matrix was increased or decreased by 20%.
- COLL(VI) & PCM ± 20%: Both alterations were applied simultaneously.

Collagen IX properties were held constant.

TABLE 2 | Extracellular matrix (ECM) and collagen type II materials properties [27, 31, 33].

Material parameters	ECM/Coll II
$\boldsymbol{E_0}$ ($\boldsymbol{MPa}$): Initial collagen coefficients	4.63 [27]
$\boldsymbol{E_\varepsilon}$ ($\boldsymbol{MPa}$): Strain-dep collagen coefficients	3670 [27]
$\boldsymbol{G_m}$ ($\boldsymbol{MPa}$): Shear modulus	0.723 [27]
$\boldsymbol{\alpha_1}$ ($\boldsymbol{MPa}$): Swelling stress coefficient	$0.4583z^2 - 0.0248z + 0.005$ [27]
$\boldsymbol{\alpha_2}$: Swelling stress coefficient	3.22 [27]
$\boldsymbol{k_0}$ ($\boldsymbol{mm^4/Ns}$)$\boldsymbol{10^{-15}}$: Zero-strain permeability	$6.7179z + 0.1016$ [27, 31]
$\boldsymbol{M}$: Material constant	$10.484z^2 - 13.644z + 8.6395$ [27, 31]
Fibril horizontal volume fraction:	15% [33]
Fibril Random volume fraction:	18% [33]
Fibril Vertical volume fraction:	21% [33]

*z: Normalized depth of the articular cartilage (starting from the cartilage-bone junction area).

TABLE 3 | Cell, territorial matrix (TM), pericellular matrix (PCM), and collagen (VI and XI) materials properties [3, 4, 15, 18, 26, 27, 31, 33, 34].

Material parameters	PCM/Coll VI	TM/Coll IX	Cell
$E_0(MPa)$: Initial collagen coefficients	0.2*ECM [4, 18]	0.2*ECM$^+$	—
$E_\varepsilon(MPa)$: Strain-dep collagen coefficients	0.2*ECM [4, 18]	0.2*ECM$^+$	—
$G_m(MPa)$: Shear modulus	0.2*ECM [3, 4]	0.2*ECM [3, 4]	0.1*ECM [3, 4]
$\alpha_1(MPa)$: Swelling stress coefficient	ECM [18]	ECM [18]	ECM (z = 0) [18]
α_2: Swelling stress coefficient	1.119*ECM [18]	1.119*ECM [18]	ECM [18]
$k_0(mm^4/Ns)10^{-15}$: Zero-strain permeability	0.2*ECM [4]	0.2*ECM [4]	0.01*ECM [4]
M: Material constant	0.2*ECM [4]	0.2*ECM [4]	—
Fibril horizontal volume fraction:	0.7*ECM [15, 26, 34]	0.1*ECM$^+$	—
Fibril Random volume fraction:	0.7*ECM [15, 26, 34]	0.1*ECM$^+$	—
Fibril Vertical volume fraction:	0.7*ECM [15, 26, 34]	0.1*ECM$^+$	—

*ECM, equivalent value assigned for ECM in Table 2.
+Determined based on the assumption of similarity to the collagen type VI; please see the limitation section in the discussion.

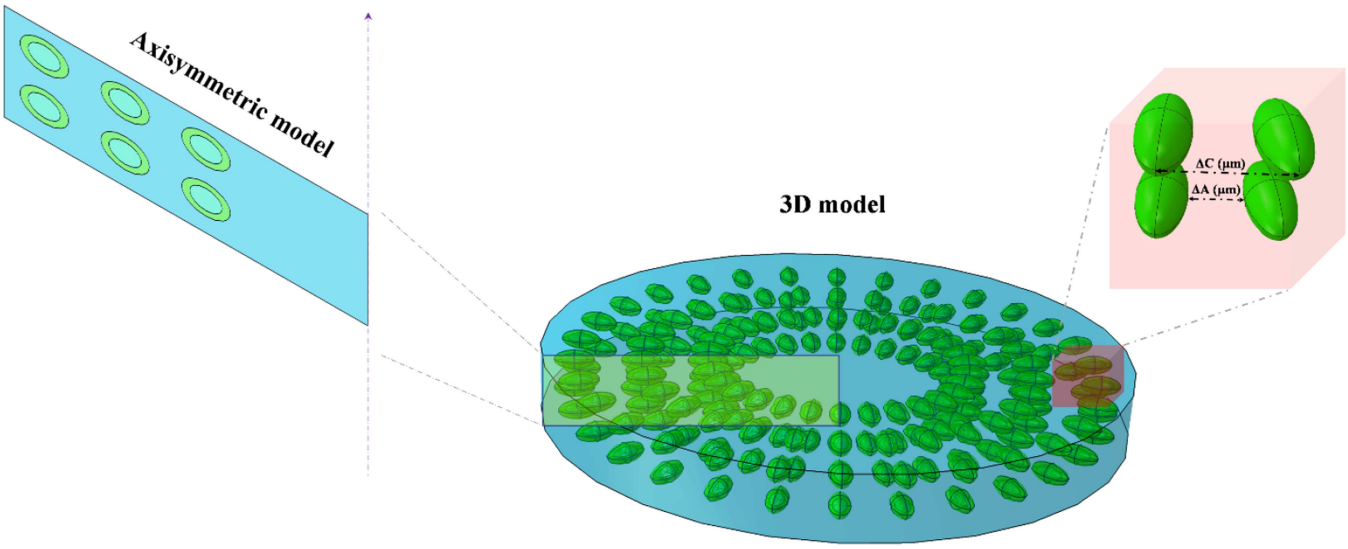

FIGURE 3 | The models (axisymmetric and 3D) employed to test the validity of the axisymmetric approach, ΔC (μm) and ΔA (μm), are the distance separating the centers of two successive cells in the circumferential direction and the proximity distance, respectively.

2.4 | Data Analysis and Validation of Axisymmetric Assumption

Chondrocyte mechanical response was quantified by: 1) total circumferential force (sum of nodal forces at the cell-PCM interface), and 2) volumetric strain. Data from all 561 cells were grouped by category (Ref, COLL(VI) ± 20%, PCM ± 20%, COLL (VI) & PCM ± 20%). Paired-sample *t*-tests ($\alpha = 0.05$) compared each altered category to the Ref case at peak load.

A recognized limitation of the axisymmetric approach is that the 3D extrusion of off-axis ellipsoidal cells results in a toroidal (donut) shape rather than a true ellipsoid. To quantify the error introduced by this geometric simplification, a separate validation study was conducted. A small-scale 3D model containing six circumferentially distributed, true ellipsoidal chondrons was compared to its axisymmetric counterpart under identical loading and material alterations (COLL(VI) ± 20%) (Figure 3). The relative error in predicted cell forces, volume changes, and von Mises stress was calculated as a function of intercellular distance in the circumferential direction (ΔC) and the lateral proximity between chondrons (ΔA). Results indicated that for intercellular distances representative of physiological cell densities (7–19 μm) [13], the error in cellular-scale outputs was between 5% and 8% (Figures 4 and 5), supporting the use of the axisymmetric model for the present comparative study.

3 | Results

3.1 | Aggregate Tissue Response

The model's prediction of axial reaction force during unconfined compression aligned with the experimental range reported by DiSilvestro and Suh [35], though it tended toward the lower bound of the experimental data (Fig. 6a). Alterations to PCM constituents modified the tissue's aggregate stiffness (Figure 3b). A 20% increase in collagen VI stiffness increased the peak reaction force by approximately 18%, while a 20% decrease reduced it by ~13%. Changes to the non-fibrillar PCM

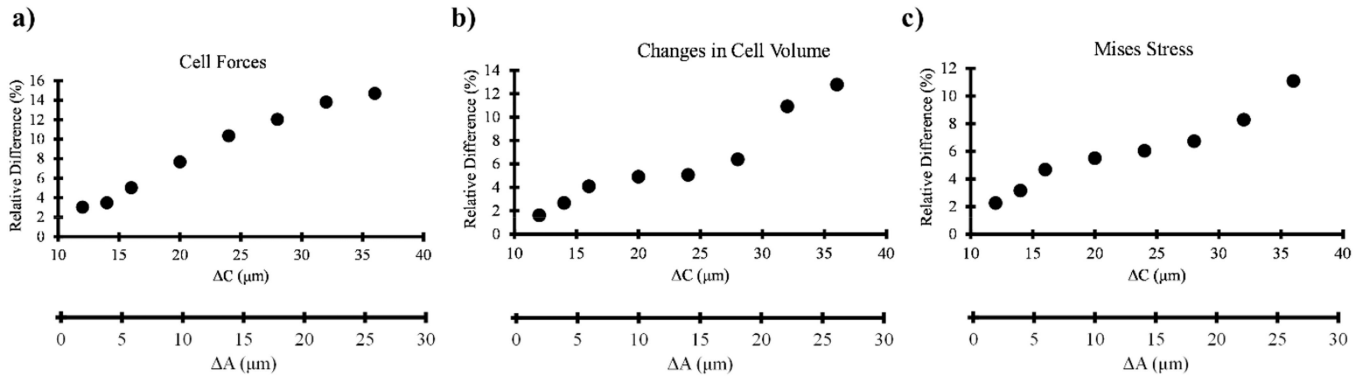

FIGURE 4 | The relative differences (error) between 3D and axisymmetric model predictions (cell forces [a], cell volume changes [b], and maximum mises stresses [c]) as a function of the distance separating the centers of two successive cells in the circumferential direction (ΔC (μm)) or the proximity distance (ΔA (μm)).

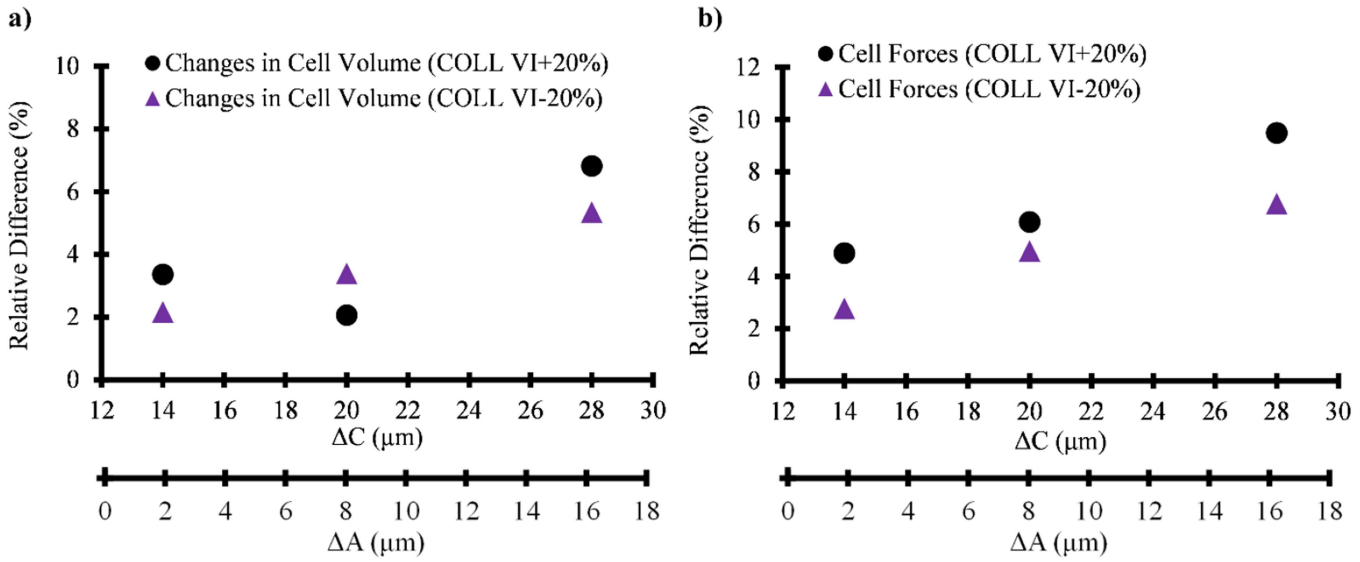

FIGURE 5 | The relative differences (error) between 3D and axisymmetric model predictions (changes in cell forces and cell volume changes due to altered collagen VI stiffness (+−30%)) as a function of the distance separating the centers of two successive cells in the circumferential direction (ΔC (μm)) or the proximity distance (ΔA (μm)).

matrix stiffness had a more moderate effect, altering the peak force by ±~4%. The simultaneous alteration of both components produced an effect similar to altering collagen VI alone, suggesting collagen VI dominates the PCM's contribution to macroscopic stiffness under this loading mode.

The time-dependent nonlinearities evident in Figure 6, including the superlinear rise in reaction force during the ramp phase and the characteristic exponential decay during stress relaxation, arise from three coupled, physically distinct mechanisms inherent to the constitutive framework. First, and most prominently, biphasic fluid–solid interactions dominate: during ramp loading, interstitial fluid pressurization transiently increases apparent tissue stiffness; as fluid redistributes and exudes through the free lateral surface during stress relaxation, load progressively transfers to the solid matrix, generating the characteristic relaxation curve. Second, the strain-dependent permeability function $k = k_0[(1+e)/(1+e_0)]^M$ causes permeability to decrease as void ratio decreases with tissue compression, progressively impeding fluid efflux and amplifying rate dependency in the mid-ramp phase. Third, the nonlinear strain-stiffening fibril constitutive law (Equation 1) causes progressive recruitment of horizontal superficial-zone collagen II fibrils as lateral strain develops under unconfined compression, contributing to the superlinear stiffness increase before relaxation onset. The superposition of these three mechanisms produces the composite nonlinear time-history observed in Figure 6, which is consistent with previously published fibril-reinforced biphasic models of articular cartilage [27, 31].

3.2 | Chondrocyte Circumferential Force

In the reference case, the total circumferential force sustained by chondrocytes was depth-dependent, highest in the superficial zone (81 ± 23 nN) and lowest in the deep zone (1.33 ± 0.6 nN) (Figure 7). Forces also decreased radially from the symmetry axis. Alterations to PCM properties significantly changed these cellular loads (Figure 4). A 20% increase in collagen VI stiffness decreased average cell forces by up to 29% in the

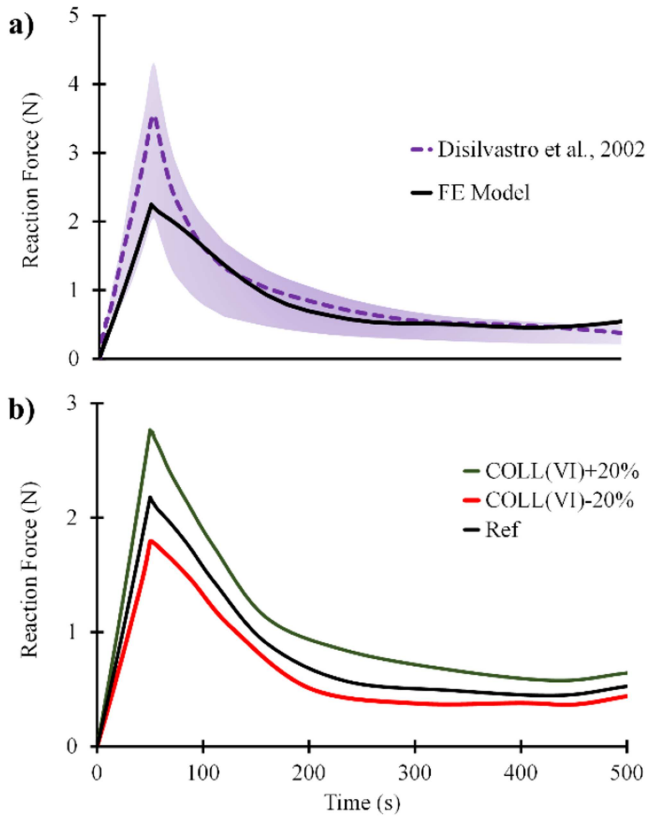

FIGURE 6 | (a) Axial reaction forces measured from unconfined compression test [20] along with FE model predictions. The highlighted area indicates the standard deviation. The non-linear rise in reaction force during the ramp phase and the subsequent exponential stress relaxation arise from three coupled mechanisms: (i) biphasic fluid pressurization and time-dependent exudation through the free lateral surface, (ii) strain-dependent permeability reduction as void ratio decreases under compression, and (iii) progressive nonlinear recruitment of tension-only horizontal collagen II fibrils in the superficial zone under lateral expansion. These mechanisms are intrinsic to the fibril-reinforced biphasic constitutive framework and are consistent with previously published models [27, 31]. (b) Predicted axial reaction forces for normal and altered collagen VI and PCM matrix stiffness (±20%), illustrating the dominant contribution of collagen VI to macroscopic tissue stiffness.

superficial zone ($p < 0.001$). A 20% decrease in collagen VI stiffness increased cell forces by up to 33% ($p < 0.001$). Changes in PCM matrix stiffness produced smaller but still significant effects, altering forces by ±~8%–12% in the superficial zone ($p < 0.01$). The radial gradient of cell forces was maintained but shifted in magnitude across all scenarios.

The pronounced depth-dependent nonlinear gradients in both Figures 7 and 8 are direct emergent consequences of five depth-stratified structural and material properties explicitly implemented in the model. (1) Collagen II fibril architecture: horizontal fibrils in the superficial zone are recruited in tension under lateral expansion during unconfined compression, generating substantial circumferential forces at the cell-PCM interface; vertical deep-zone fibrils resist axial compression with far less lateral strain amplification, yielding lower circumferential loads. (2) Cell density: the higher volume fraction of cellular units in the superficial zone (~75%) concentrates load-bearing area at cell-PCM interfaces, amplifying transmitted forces per cell compared to the deep zone (~12.5%). (3) Fluid fraction gradient: a fluid content of ~85% at the articular surface versus ~70% at the subchondral boundary results in greater fluid-mediated load transfer and larger transient volumetric deformations in superficial-zone chondrocytes, consistent with the ~18% versus ~4% volumetric changes observed. (4) Depth-dependent permeability: the lower void ratio and higher tissue density in the deep zone retard fluid exudation, shifting more load to the solid matrix and reducing fluid-driven cell deformation. (5) Unconfined compression strain field: the free lateral boundary produces both axial and lateral strain gradients, with the superficial zone experiencing the highest multiaxial strain amplitudes due to proximity to the loading platen. The depth-dependent nonlinearity in Figures 7 and 8 therefore reflects the mechanically realistic, explicitly stratified architecture of the model and is consistent with experimental observations of depth-dependent chondrocyte deformation in articular cartilage [19].

3.3 | Chondrocyte Volume Change

At peak load in the reference case, chondrocyte volumetric change ranged from ~18% in the superficial zone to ~4% in the deep zone (Figure 8). Volume changes were minimal at equilibrium. Alterations in PCM properties modulated this deformation (Figure 8). Increasing collagen VI stiffness by 20% significantly reduced volumetric change by an average of 15% in the superficial zone ($p < 0.001$). Decreasing collagen VI stiffness increased changes by ~8% ($p < 0.001$) in the superficial zone. Changes in PCM matrix stiffness had a more subdued effect, altering volume change by ±~3%–5% ($p < 0.01$ in superficial/transitional zones). Combined alterations yielded results closely aligned with the collagen VI-only case.

3.4 | Stress Distributions

At peak load, the von Mises stress distribution was analyzed in a representative sub-region located near the symmetry axis in the superficial zone (Figure 9). This region was selected because it experiences the highest multiaxial strain amplitudes under unconfined compression and is therefore the most mechanobiologically critical area for chondrocyte loading. The displayed sub-region encompasses a depth of approximately 0.1–0.2 mm from the articular surface and spans a radial width of approximately 0.3 mm from the symmetry axis; its spatial location relative to the full model domain is indicated by the inset schematic in Figure 9. Individual tissue compartments, collagen II ECM fibrils, collagen VI PCM fibrils, non-fibrillar matrices (ECM, TM, PCM), and the chondrocytes, are individually identified by labels in Figure 9a. Color contours represent von Mises stress in kPa, with the minimum and maximum values of the color scale labeled on each bar. In the reference case, collagen II fibrils supported the greatest stress, followed by collagen VI. The non-fibrillar matrices (ECM, TM, PCM) and the chondrocytes themselves sustained substantially lower stresses. Altering collagen VI stiffness redistributed stress within the PCM and to the chondrocyte (Figure 10). Figure 10

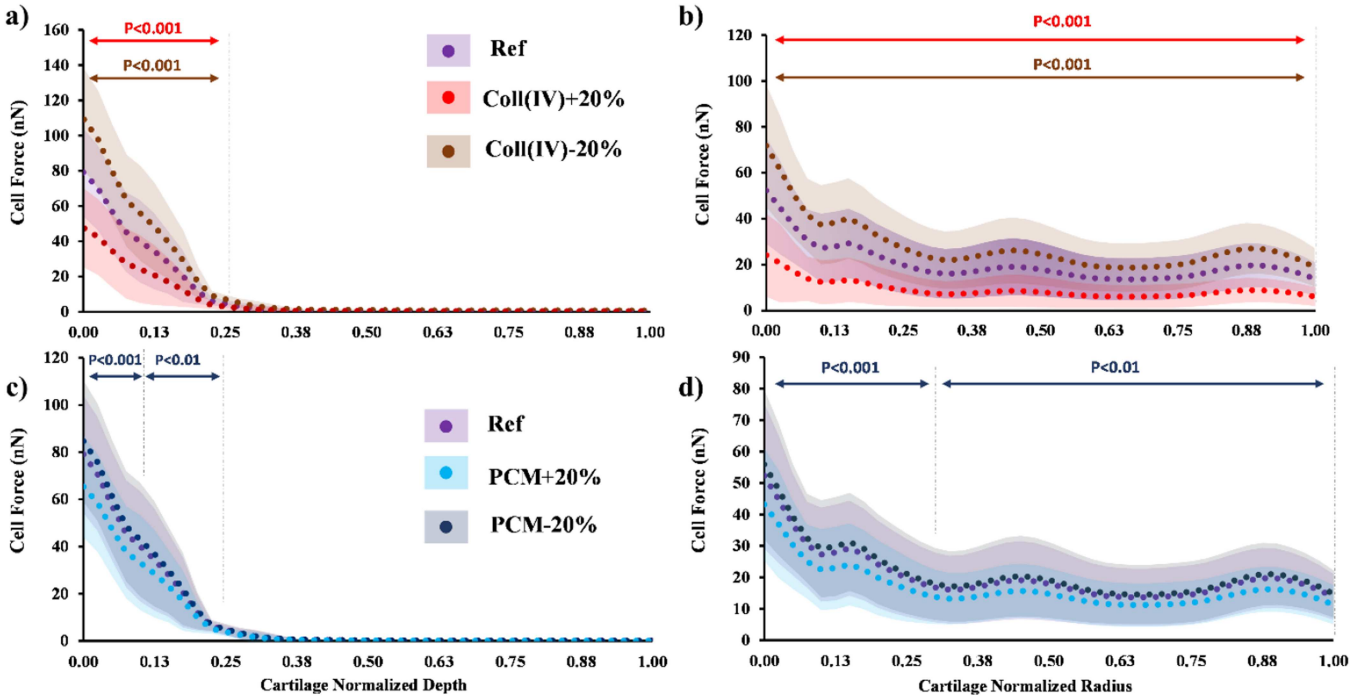

FIGURE 7 | Computed total circumferential cell forces for reference (Ref) and altered collagen VI (a, b) and PCM matrix (c, d) stiffness (±20%), versus normalized cartilage depth and radius, as well as the statistical significance of the means differences (T-test, $\alpha = 0.05$). These forces were calculated by summating each cell's circumferential nodal forces (nodes in the junction between the PCM and the cell).

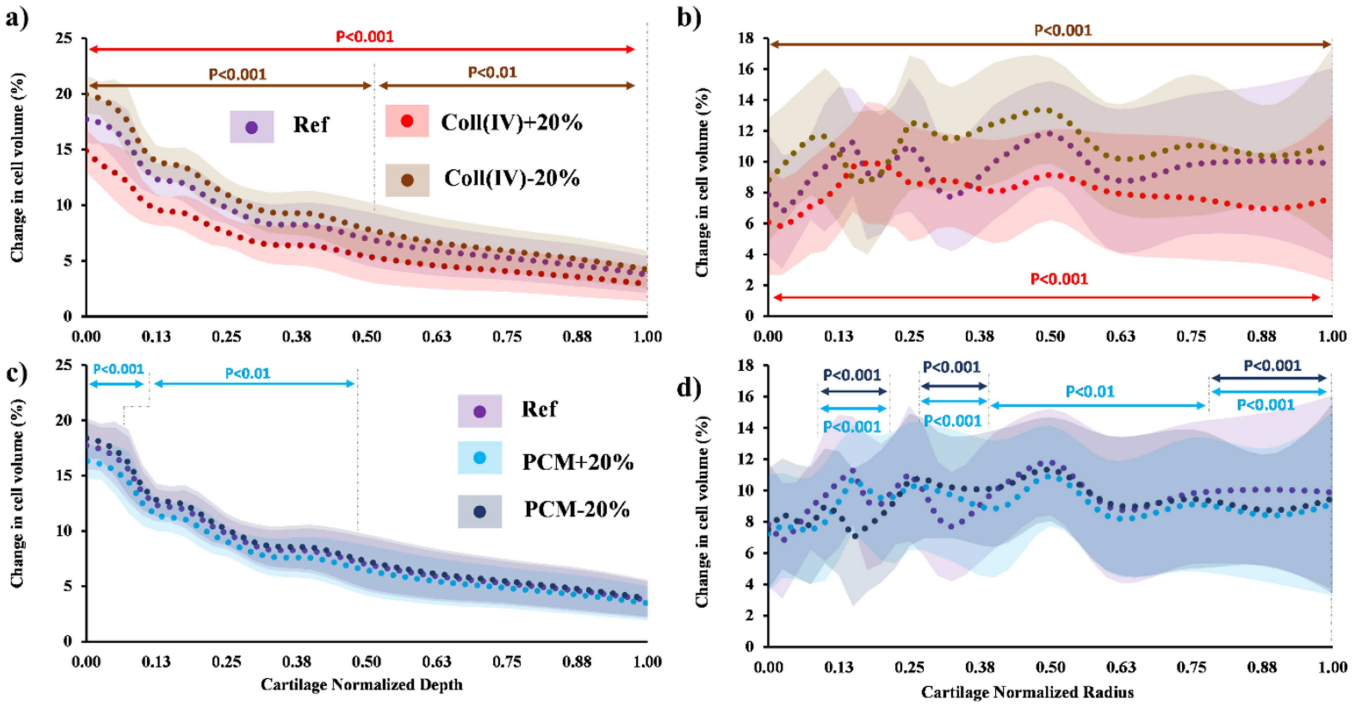

FIGURE 8 | Computed changes in cell volume for reference (Ref) and altered collagen VI (a, b) and PCM matrix (c, d) stiffness (±20%), versus normalized cartilage depth and radius, as well as the statistical significance of the means differences (T-test, $\alpha = 0.05$). The cell volume change was calculated based on the summation of change element volume (Evol) constituting the chondrocytes.

presents side-by-side von Mises stress contours for COLL (VI) − 20%, Reference, and COLL(VI) + 20% conditions, using a unified color scale across all sub-panels to facilitate direct visual comparison. Decreasing collagen VI stiffness by 20% led to a marked increase in the stress borne by the non-fibrillar PCM matrix and the chondrocyte (by ~40% and ~25%, respectively), indicating a load-sharing relationship where a weaker fibrillar network shifts stress to the ground substance and the cell.

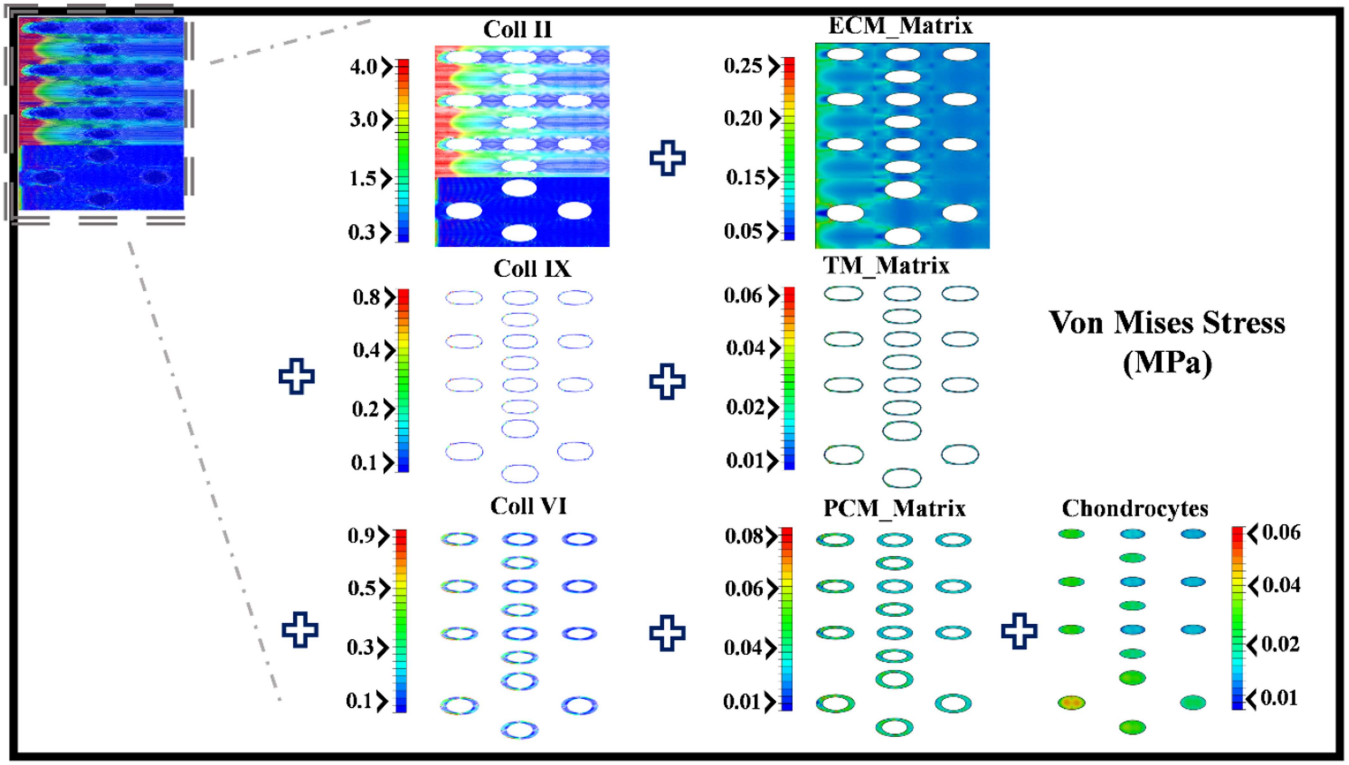

FIGURE 9 | Predicted von Mises stress distributions (kPa; color scale labeled with minimum and maximum values on each bar) over all tissue compartments at peak compressive load under the reference condition. The displayed region is a magnified sub-region located near the symmetry axis within the superficial zone (approximately 0–0.18 mm from the articular surface; approximately 0–0.30 mm radially from the axis), selected because it experiences the highest multiaxial strain amplitudes under unconfined compression and is therefore the most mechanobiologically critical area for chondrocyte loading. Its spatial location relative to the full model domain is indicated by the inset schematic. Individual tissue compartments are identified by annotated labels: fibrillar networks (collagen II ECM fibrils; collagen VI PCM fibrils; collagen IX TM fibrils) and non-fibrillar solid matrices (ECM, TM, PCM ground substance) and the chondrocyte. Collagen II fibrils sustain the highest stresses, followed by collagen VI; the non-fibrillar matrices and the chondrocytes bear substantially lower stresses under reference conditions, consistent with the load-shielding role of the fibrillar network.

4 | Discussion

This study utilized a novel, explicit multiscale computational model to dissect the mechanical roles of two key pericellular matrix (PCM) constituents-the collagen VI fibrillar network and the non-fibrillar ground substance-in articular cartilage. The central finding is that while both components influence the chondrocyte mechanical microenvironment, collagen VI stiffness is the dominant modulator of both macro-scale tissue stiffness and micro-scale cellular loading and deformation under unconfined compression. This work provides a quantitative framework linking alterations in PCM composition to changes in chondrocyte mechanobiological stimuli.

Our model's prediction of tissue reaction force validated against independent experimental data [20], though it slightly underestimated the peak response. This may stem from parameter choices optimized from macro-model studies [27] or simplifications in representing the full heterogeneity of the collagen-proteoglycan matrix. Nevertheless, the model successfully captured the transient and equilibrium phases of the biphasic response. The significant sensitivity of tissue stiffness to collagen VI alterations (±20% change yielding ~±15% force change) aligns with its postulated role as a mechanical stabilizer of the chondron [3, 5, 14, 35]. In contrast, the non-fibrillar PCM matrix, while influential, had a more tempered effect on macro-mechanics. This may reflect its primary role in regulating local fluid flow and osmotic environment rather than bearing significant axial load under compression [4, 16]. The finding that combined alteration produced no synergistic effect suggests the collagen VI network carries the primary load within the PCM under this specific loading configuration.

At the cellular level, the inverse relationship between collagen VI stiffness and both chondrocyte force and deformation highlights its function as a protective "shielding" element. A stiffer collagen VI network appears to divert more load around the cell, reducing its mechanical burden. This is mechanistically consistent with studies showing that compromised collagen VI leads to increased chondrocyte deformation and altered biosynthetic activity [13, 36]. The stress distribution results (Figures 9 and 10) visually confirm this load transfer: weakening collagen VI increases stress on both the PCM ground substance and the chondrocyte itself. This redistribution could have significant mechanobiological consequences, potentially over-activating ion channels like TRPV4, which are sensitive to membrane strain and osmolarity, and dysregulating downstream calcium signaling and metabolic pathways [37–42]. The more modest effect of altering the PCM ground substance stiffness suggests its role is more nuanced, possibly related to

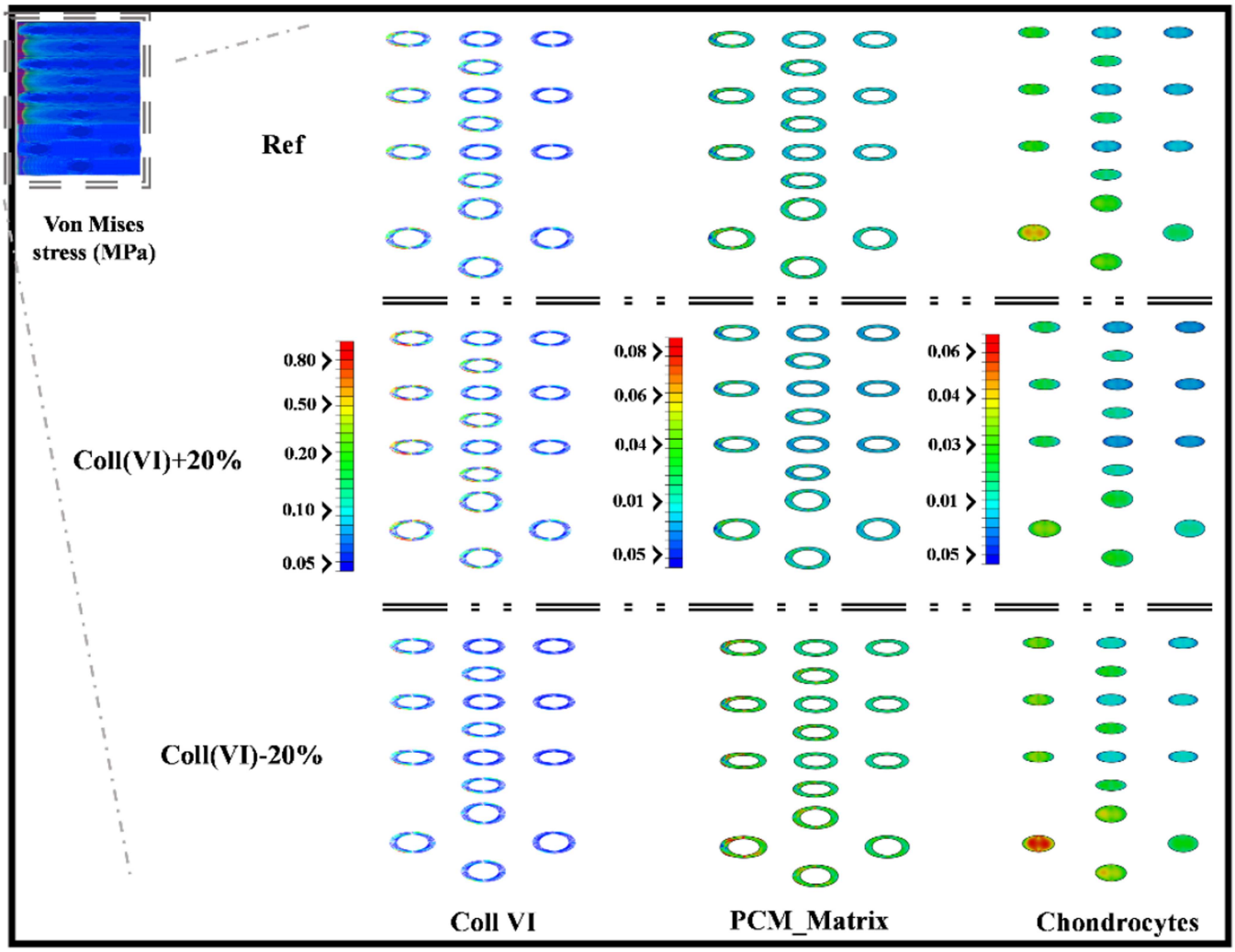

FIGURE 10 | Predicted von Mises stress distributions (kPa; unified color scale with labeled minimum and maximum values applied consistently across all sub-panels) over the fibrillar (collagen VI) and non-fibrillar components of the PCM, as well as the chondrocyte, in the same superficial-zone sub-region depicted in Figure 9, under three conditions presented side-by-side: COLL(VI) − 20% (left), Reference (center), and COLL(VI) + 20% (right). Each sub-panel is labeled with its condition. Decreasing collagen VI stiffness by 20% markedly increases the stress borne by the non-fibrillar PCM matrix (~40% increase) and the chondrocyte (~25% increase) relative to the reference, demonstrating a load-sharing mechanism whereby a weaker fibrillar network redistributes mechanical load to the proteoglycan-rich ground substance and the cell. Increasing collagen VI stiffness produces the inverse redistribution.

modulating the fluid pressure and osmotic gradients within the PCM that influence cell volume regulation and solute transport [4, 16]. This distinction underscores the importance of modeling the PCM as a composite of distinct fibrillar and non-fibrillar phases.

A key strength of this study is the explicit, concurrent multi-scale approach, which minimizes assumptions associated with homogenization or sequential sub-modeling techniques [18, 27, 43]. By solving the macro- and micro-mechanics simultaneously, the model captures the continuous feedback between cell deformation and matrix stress. Our validation study against a 3D benchmark confirms that the axisymmetric simplification, while introducing a quantifiable geometric error (5%–8% for key cellular outputs), remains a viable strategy for comparative parametric studies, especially given the prohibitive computational cost of a full 3D explant model with anatomical cell density.

Several limitations warrant mention. First, the 20% alteration in properties, while physiologically plausible, is parametric; a wider sensitivity analysis would be valuable but computationally expensive. Second, collagen VI was modeled with random in-plane orientation, whereas some studies suggest a more circumferential organization [3]; future work should examine the sensitivity of results to fibril architecture. Third, the model assumes identical constitutive behavior for collagen VI and the PCM matrix across all cartilage zones, though zonal variations may exist. Fourth, the loading rate was slow (0.001/s), limiting fluid pressurization; faster, more physiological rates may amplify the role of the PCM's permeability and its non-fibrillar matrix. Fifth, the chondrocyte was modeled as a homogeneous, poro-hyperelastic solid, neglecting intracellular structures (cytoskeleton, nucleus) that contribute to its mechanical behavior [44]. Sixth, chondrocyte morphology was modeled as uniform mildly oblate ellipsoids across all depth zones, whereas experimental measurements show a transition

from highly flattened superficial cells to near-spherical deep-zone cells [19]. While this simplification was adopted to isolate the effects of PCM constituent properties from confounding morphological variables, implementing zone-specific cell geometries may further refine cellular-scale predictions and is an important direction for future work. Seventh, while the pre-swelling equilibration step was performed to establish physiologically consistent fibril pre-stress, consistent with the Wilson et al. framework [27, 28], the sensitivity of model outputs to alternative swelling coefficient values was not fully explored; future studies should quantify this sensitivity, particularly for PCM constituents where osmotic properties are less well characterized.

Finally, while the axisymmetric validation provides confidence, the gold standard remains a full 3D model. Future advances in computational power and meshing algorithms should make this feasible, enabling investigation of more complex loading (e.g., shear, rolling) where 3D cell shape and adjacency are critical.

5 | Conclusion

This multiscale 'in silico' investigation demonstrates that the pericellular matrix acts as a critical mechanical filter for chondrocytes, with its collagen VI fibrillar network being the primary determinant of load transfer at both the tissue and cellular scale under compression. Alterations in collagen VI stiffness, more so than changes in the non-fibrillar PCM matrix, significantly modulate chondrocyte stress and strain, potentially disrupting normal mechanotransduction pathways. The developed modeling framework offers a powerful tool for probing structure-function relationships in cartilage and for predicting how degradation of specific matrix components, as occurs in injury or early osteoarthritis, compromises tissue integrity from the cellular level upward.

Author Contributions

All authors have read and approved this submission; the first author carried out analyses, all participated in the definition, design, and development of the work, and finally, the manuscript was written by all authors.

Acknowledgments

The authors would like to thanks editors for their support and guidance. The work is supported by a grant from the Kuwait Foundation for the Advancement of Sciences [CN22-13BP-1706].

Conflicts of Interest

The authors declare no conflicts of interest.

Data Availability Statement

Data sharing not applicable to this article as no datasets were generated or analyzed during the current study.

References

1. A. J. Sophia Fox, A. Bedi, and S. A. Rodeo, "The Basic Science of Articular Cartilage: Structure, Composition, and Function," *Sports Health* 1 (2009): 461–468.

2. H. Gahunia, A. Gross, K. Pritzker, P. Babyn, and L. Murnaghan, "*Articular Cartilage of the Knee*,". Health, Disease and Therapy Springer, (2020), https://www.springer.com/gp/book/9781493975853.

3. R. E. Wilusz, J. Sanchez-Adams, and F. Guilak, "The Structure and Function of the Pericellular Matrix of Articular Cartilage," *Matrix Biology* 39 (2014): 25–32.

4. F. Guilak, L. G. Alexopoulos, M. L. Upton, et al., "The Pericellular Matrix as a Transducer of Biomechanical and Biochemical Signals in Articular Cartilage," *Annals of the New York Academy of Sciences* 1068 (2006): 498–512.

5. N. A. Zelenski, H. A. Leddy, J. Sanchez-Adams, et al., "Type Vi Collagen Regulates Pericellular Matrix Properties, Chondrocyte Swelling, and Mechanotransduction in Mouse Articular Cartilage," *Arthritis Rheumatol* 67 (2015): 1286–1294.

6. V. C. Mow and X. E. Guo, "Mechano-Electrochemical Properties of Articular Cartilage: Their Inhomogeneities and Anisotropies," *Annual Review of Biomedical Engineering* 4 (2002): 175–209.

7. M. Knight, S. Ghori, D. Lee, and D. Bader, "Measurement of the Deformation of Isolated Chondrocytes in Agarose Subjected to Cyclic Compression," *Medical Engineering & Physics* 20 (1998): 684–688.

8. M. B. Goldring, *Articular Cartilage Degradation In Osteoarthritis* (SAGE Publications Sage CA, 2012).

9. P. Gratal, A. Mediero, O. Sánchez-Pernaute, et al., "Chondrocyte Enlargement Is a Marker of Osteoarthritis Severity," *Osteoarthritis and Cartilage* 27 (2019): 1229–1234.

10. J. Sanchez-Adams, H. A. Leddy, A. L. McNulty, C. J. O'Conor, and F. Guilak, "The Mechanobiology of Articular Cartilage: Bearing the Burden of Osteoarthritis," *Current Rheumatology Reports* 16 (2014): 451.

11. L. G. Alexopoulos, I. Youn, P. Bonaldo, and F. Guilak, "Developmental and Osteoarthritic Changes in Col6a1-knockout Mice: Biomechanics of Type Vi Collagen in the Cartilage Pericellular Matrix," *Arthritis & Rheumatism: Official Journal of the American College of Rheumatology* 60 (2009): 771–779.

12. P. Bonaldo, V. Russo, F. Bucciotti, R. Doliana, and A. Colombatti, "Structural and Functional Features of the Alpha 3 Chain Indicate a Bridging Role for Chicken Collagen Vi in Connective Tissues," *Biochemistry* 29 (1990): 1245–1254.

13. K. D. Jadin, B. L. Wong, W. C. Bae, et al., "Depth-Varying Density and Organization of Chondrocytes in Immature and Mature Bovine Articular Cartilage Assessed by 3d Imaging and Analysis," *Journal of Histochemistry & Cytochemistry* 53 (2005): 1109–1119.

14. K. Hu, L. Xu, L. Cao, et al., "Pathogenesis of Osteoarthritis-Like Changes in the Joints of Mice Deficient in Type Ix Collagen," *Arthritis & Rheumatism* 54 (2006): 2891–2900.

15. B. J. Bielajew, J. C. Hu, and K. A. Athanasiou, "Collagen: Quantification, Biomechanics and Role of Minor Subtypes in Cartilage," *Nature Reviews Materials* 5 (2020): 1–18.

16. C. Canal Guterl, C. T. Hung, and G. A. Ateshian, "Electrostatic and Non-Electrostatic Contributions of Proteoglycans to the Compressive Equilibrium Modulus of Bovine Articular Cartilage," *Journal of Biomechanics* 43 (2010): 1343–1350.

17. P. Julkunen, W. Wilson, H. Isaksson, J. S. Jurvelin, W. Herzog, and R. K. Korhonen, "A Review of the Combination of Experimental Measurements and Fibril-Reinforced Modeling for Investigation of Articular Cartilage and Chondrocyte Response to Loading," *Computational and Mathematical Methods in Medicine* (2013): 326150.

18. P. Tanska, M. S. Venäläinen, A. Erdemir, and R. K. Korhonen, "A Multiscale Framework for Evaluating Three-Dimensional Cell Mechanics in Fibril-Reinforced Poroelastic Tissues With Anatomical Cell Distribution – Analysis of Chondrocyte Deformation Behavior in Mechanically Loaded Articular Cartilage," *Journal of Biomechanics* 101 (2020): 109648.

19. I. Youn, J. B. Choi, L. Cao, L. A. Setton, and F. Guilak, "Zonal Variations in the Three-Dimensional Morphology of the Chondron Measured In Situ Using Confocal Microscopy," *Osteoarthritis and Cartilage* 14 (2006): 889–897.

20. M. R. DiSilvestro and J. K. Suh, "Biphasic Poroviscoelastic Characteristics of Proteoglycan-Depleted Articular Cartilage: Simulation of Degeneration," *Annals of Biomedical Engineering* 30 (2002): 792–800.

21. R. S. Gilmore and A. J. Palfrey, "Chondrocyte Distribution in the Articular Cartilage of Human Femoral Condyles," *Journal of Anatomy* 157 (1988): 23–31.

22. M. Adouni, A. Shirazi-Adl, and R. Shirazi, "Computational Biodynamics of Human Knee Joint in Gait: From Muscle Forces to Cartilage Stresses," *Journal of Biomechanics* 45 (2012): 2149–2156.

23. R. Shirazi and A. Shirazi-Adl, "Analysis of Articular Cartilage as a Composite Using Nonlinear Membrane Elements for Collagen Fibrils," *Medical Engineering & Physics* 27 (2005): 827–835.

24. R. Shirazi, A. Shirazi-Adl, and M. Hurtig, "Role of Cartilage Collagen Fibrils Networks in Knee Joint Biomechanics under Compression," *Journal of Biomechanics* 41 (2008): 3340–3348.

25. X. Bi, X. Yang, M. P. Bostrom, and N. P. Camacho, "Fourier Transform Infrared Imaging Spectroscopy Investigations in the Pathogenesis and Repair of Cartilage," *Biochimica et Biophysica Acta/General Subjects* 1758 (2006): 934–941.

26. M. Khoshgoftar, P. A. Torzilli, and S. A. Maher, "Influence of the Pericellular and Extracellular Matrix Structural Properties on Chondrocyte Mechanics," *Journal of Orthopaedic Research®* 36 (2018): 721–729.

27. S. S. Sajjadinia, M. Haghpanahi, and M. Razi, "Computational Simulation of the Multiphasic Degeneration of the Bone-Cartilage Unit During Osteoarthritis via Indentation and Unconfined Compression Tests," *Proceedings of the Institution of Mechanical Engineers, Part H: Journal of Engineering in Medicine* 233 (2019): 871–882.

28. W. Wilson, J. M. Huyghe, and C. C. van Donkelaar, "Depth-Dependent Compressive Equilibrium Properties of Articular Cartilage Explained by Its Composition," *Biomechanics and Modeling in Mechanobiology* 6 (2007): 43–53.

29. W. M. Lai, V. C. Mow, and V. Roth, "Effects of Nonlinear Strain-Dependent Permeability and Rate of Compression on the Stress Behavior of Articular Cartilage," *Journal of Biomechanical Engineering* 103 (1981): 61–66.

30. P. J. Prendergast, W. D. van Driel, and J.-H. Kuiper, "A Comparison of Finite Element Codes for the Solution of Biphasic Poroelastic Problems," *Proceedings of the Institution of Mechanical Engineers, Part H: Journal of Engineering in Medicine* 210 (1996): 131–136.

31. W. Wilson, C. C. van Donkelaar, B. van Rietbergen, K. Ito, and R. Huiskes, "Stresses in the Local Collagen Network of Articular Cartilage: A Poroviscoelastic Fibril-Reinforced Finite Element Study," *Journal of Biomechanics* 37 (2004): 357–366.

32. R. S. Aghjari, *Computational Biomechanics of the Human Knee Joint: Role of Collagen Fibrils Networks* (ProQuest, 2008).

33. R. Shirazi and A. Shirazi-Adl, "Deep Vertical Collagen Fibrils Play a Significant Role in Mechanics of Articular Cartilage," *Journal of Orthopaedic Research* 26 (2008): 608–615.

34. L. Alcaide-Ruggiero, V. Molina-Hernández, M. M. Granados, and J. M. Domínguez, "Main and Minor Types of Collagens in the Articular Cartilage: The Role of Collagens in Repair Tissue Evaluation in Chondral Defects," *International Journal of Molecular Sciences* 22 (2021): 13329.

35. Y. Luo, D. Sinkeviciute, Y. He, et al., "The Minor Collagens in Articular Cartilage," *Protein & Cell* 8 (2017): 560–572.

36. S. Roa, N. Haberkorn, and M. Sirena, "Atomic Force Microscopy Nano-Indentation for Testing Mechanical Properties in Thin Films," *Materials Today: Proceedings* 14 (2019): 113–116.

37. P.-hG. Chao, A. C. West, and C. T. Hung, "Chondrocyte Intracellular Calcium, Cytoskeletal Organization, and Gene Expression Responses to Dynamic Osmotic Loading," *American Journal of Physiology-Cell Physiology* 291 (2006): C718–C725.

38. G. Erickson, D. Northrup, and F. Guilak, "Hypo-Osmotic Stress Induces Calcium-Dependent Actin Reorganization in Articular Chondrocytes," *Osteoarthritis and Cartilage* 11 (2003): 187–197.

39. M. A. Haider, R. C. Schugart, L. A. Setton, and F. Guilak, "A Mechano-Chemical Model for the Passive Swelling Response of An Isolated Chondron Under Osmotic Loading," *Biomechanics and Modeling in Mechanobiology* 5 (2006): 160–171.

40. A. Maroudas, "Physico-chemical Properties of Articlar Cartilage," in *Adlt articular cartilage* edited by Freeman MAR (Pitman Medical, Tunbridge Wells, 1979): 215–290.

41. A. L. Clark, B. J. Votta, S. Kumar, W. Liedtke, and F. Guilak, "Chondroprotective Role of the Osmotically Sensitive Ion Channel Transient Receptor Potential Vanilloid 4: Age-And Sex-Dependent Progression of Osteoarthritis in Trpv4-deficient Mice," *Arthritis & Rheumatism* 62 (2010): 2973–2983.

42. C. J. O'Conor, H. A. Leddy, H. C. Benefield, W. B. Liedtke, and F. Guilak, "TRPV4-mediated Mechanotransduction Regulates the Metabolic Response of Chondrocytes to Dynamic Loading," *Proceedings of the National Academy of Sciences* 111 (2014): 1316–1321.

43. S. C. Sibole and A. Erdemir, "Chondrocyte Deformations as a Function of Tibiofemoral Joint Loading Predicted by a Generalized High-Throughput Pipeline of Multi-Scale Simulations," *PLoS One* 7 (2012): e37538.

44. A. C. Shieh and K. A. Athanasiou, "Principles of Cell Mechanics for Cartilage Tissue Engineering," *Annals of Biomedical Engineering* 31 (2003): 1–11.